Measurement of the oscillator strength distribution in helium

Shahid Hussain, M. Saleem, and M. A. Baig*
Atomic and Molecular Physics Laboratory, Department of Physics, Quaid-i-Azam University, Islamabad 45320, Pakistan
(Received 17 March 2007; published 2 July 2007)

The oscillator strength distribution in the discrete and continuous regions of the spectrum of helium from the $2s\ ^1S_0$ metastable state has been determined using a Nd: yttrium aluminum garnet (YAG) pumped dye laser system in conjunction with a low pressure rf glow discharge. The saturation technique has been employed to determine the photoionization cross section from the $2s\ ^1S_0$ excited state at and above the first ionization threshold. The measured value of the photoionization cross section at the ionization threshold has been used to extract the f values for the $2s\ ^1S \rightarrow np\ ^1P$ Rydberg series from $n=10$ to $n=52$. The f values of the observed Rydberg series decrease smoothly with an increase of the principal quantum number. In the continuum region the oscillator strength densities have been estimated by measuring the photoionization cross sections from the $2s\ ^1S_0$ excited state at five ionizing laser wavelengths above the first ionization threshold. The discrete f values smoothly merge into the continuous oscillator strength densities across the ionization threshold.

DOI: 10.1103/PhysRevA.76.012701 PACS number(s): 32.80.Fb, 32.80.Rm, 32.80.Cy

I. INTRODUCTION

The dipole oscillator strength distribution as a function of excitation energy is an important property of an atom or molecule [1], which directly determines the photoabsorption cross sections in the discrete region, whereas in the continuum it yields the absolute value of the photoionization cross section [2]. The absolute dipole oscillator strengths for optical electronic excitations from the ground state of helium provide a stringent test for quantum mechanical calculations and for the evaluation of the most accurate correlated wave functions for the two-electron atomic system. However, little experimental data are available for the transitions starting from the ground state or from the lower excited states of helium. This is because most of the optically based techniques (e.g., lifetimes, level crossing, Hanle effect, self-absorption, etc.) to measure the discrete oscillator strengths are very difficult and also not readily applicable to the higher excited states [3–5]. Chan *et al.* [6] experimentally determined the absolute optical oscillator strengths for the helium $1s\ ^1S \rightarrow n\ ^1P$ $(n=2-7)$ transitions using dipole (e,e) spectroscopy at high energy resolution. Subsequently, Chan *et al.* [7] determined the absolute optical oscillator strengths for helium excitations $1\ ^1S \rightarrow n\ ^1P$, $n=2-7$ using the technique that utilizes the virtual-photon field of a fast electron inelastically scattered at negligible momentum transfer. The only reported experimental values of oscillator strengths for the $2s\ ^{1,3}S \rightarrow n\ ^{1,3}P$ Rydberg series of helium are those by Dunning and Stebbings [8] who determined the f values for the first three members of the series using the saturation technique. Besides these few experimental attempts, mostly the theoretical efforts have been devoted to determine reliable atomic oscillator strengths (f values) of helium and helium-like ions. Various authors have computed the f values for the transitions between S and P states of helium and of helium-like atoms using different types of approximate wave functions. Green *et al.* [9,10] calculated the f values for the $m\ S \rightarrow nP$ transitions in helium with the help of configuration-interaction calculation. Wiese *et al.* [11] compiled the oscillator strength data for the $1\ ^1S \rightarrow n\ ^1P$, $n \leqslant 12$ and $2\ ^1S \rightarrow n\ ^1P$, $n \leqslant 10$ Rydberg series of helium. Schiff *et al.* [12] computed the f values for the $m\ ^{1,3}S \rightarrow n\ ^{1,3}P$ transitions with $m,n \leqslant 5$ for members of the helium isoelectronic sequence up to $Z=10$. Devine and Stewart [13] calculated the optical dipole oscillator strengths between the $1\ ^1S$, $2\ ^{1,3}S$, $2\ ^{1,3}P$, $3\ ^{1,3}S$, $3\ ^{1,3}P$, and $3\ ^{1,3}D$ states of helium using perturbation theory. Amusia and Cherepkov [14] calculated the photoionization cross sections and the oscillator strengths for helium, lithium, and beryllium in the framework of the random-phase approximation with exchange (RPAE). Davis and Chung [15] calculated the energy, wave function, oscillator strength, radial expectation integrals, and mass-polarization effect of the $1s\ ^1S$, $1s\ 2s\ ^{1,3}S$, $1s\ 2p\ ^{1,3}P$, and $1s\ 3d\ ^{1,3}D$ states of helium using simple configuration-interaction basis functions. Kono and Hattori [16] calculated the oscillator strengths for all the allowed transitions between the states $n\ ^{1,3}S$, $n\ ^{1,3}P$, and $n\ ^{1,3}D$, $n \leqslant 9$ in neutral helium using variational wave functions. Subsequently, Kono and Hattori [17] calculated the oscillator strengths for the $m\ P \rightarrow n\ D$, $m,n \leqslant 5$ transitions in heliumlike ions with $Z=3-7$ using Hylleraas-type wave functions. Fernley *et al.* [18] calculated the energy, f values, and the photoionization cross section for all the bound states $1s\ n\ell$ with $n \leqslant 10$ and $\ell \leqslant 2$ of He-like ions. Chen [19] calculated the transitions $m\ S \rightarrow n\ P$, $m,n \leqslant 5$ using accurate wave functions and energies of $n\ ^{1,3}S$ and $n\ ^{1,3}P$ states of helium. Chang and Fang [20] discussed the energy dependent behavior of the photoionization cross section and oscillator strengths of the discrete transitions of He and Mg-like divalent Al^+ ion. Dillon and Inokuti [21] presented the analytic properties of the oscillator strength distribution in a single-electron continuum of an atom giving examples of H, He, Li, and Na atoms. Berkowitz [22] discussed the oscillator strength distribution in the discrete and continuous spectrum of helium and tested the available experimental and calculated photoabsorption cross sections by the sum rules.

We have experimentally determined the energy dependent behavior of the oscillator strength from the discrete to the

*Corresponding author. FAX: +92 51 9210256. baig@qau.edu.pk

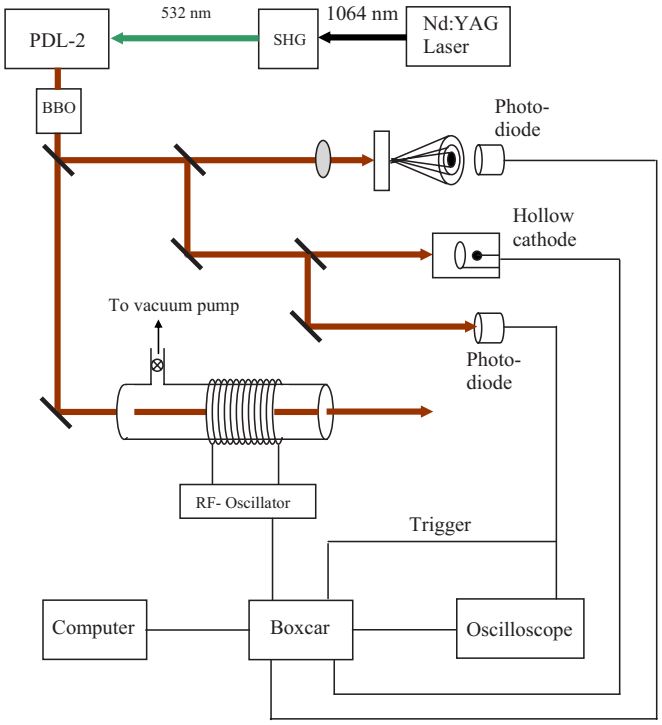

FIG. 1. (Color online) Experimental setup for the measurement of the oscillator strength distribution in helium.

continuous spectrum of helium using $2s\ ^1S_0$ as an intermediate state. In the discrete region the f values of the $2s\ ^1S \rightarrow np\ ^1P$ $(10 \leqslant n \leqslant 52)$ Rydberg series have been determined. The density of oscillator strength in the continuum have been deduced from the measured values of the photoionization cross sections corresponding to the excess energies of 0.0, 0.16, 0.3, 0.46, 0.62, and 0.69 eV, above the first ionization threshold. Continuity in the oscillator strengths has been found across the ionization threshold.

II. EXPERIMENTAL SETUP

In our previous work [23], we have presented experimental studies on the electric field measurement in glow discharges. It was inferred that a rf glow discharge, because of having low net electric field, is extremely suitable for studying the high lying Rydberg states. In addition, a low field helium glow discharge has higher density of the $2s\ ^1S_0$ metastable state [24]. Therefore for the present studies we have used a low-pressure rf glow discharge operating at a frequency of 4 MHz. The locally made rf discharge cell consists of a 120 mm long glass tube of diameter 25 mm and quartz windows at both ends. A single 24-turns copper coil was wrapped on it to produce the discharge and also to collect the optogalvanic signal [25]. The design of the rf oscillator circuit is similar to that of May and May [26], who used a 35 MHz oscillator for the laser optogalvanic studies. A schematic diagram of the experimental setup is shown in Fig. 1. The laser system was comprised of a Q-switched pulsed Nd: yttrium aluminum garnet (YAG) laser (Brilliant, Quantel) coupled with the second-harmonic generation (SHG) module for producing a laser at 532 nm capable of delivering energy of 180 mJ. The laser was operated at 10 Hz with pulse duration of $\approx$5 ns and was used to pump a commercial dye laser system (Quanta-ray, PDL-2). The line width of the dye laser was $\leqslant 0.3\ \mathrm{cm}^{-1}$. The spectral range from 312 nm to 325 nm for recording the $2s\ ^1S \rightarrow np\ ^1P$ $(10 \leqslant n \leqslant 52)$ Rydberg series of helium was covered by charging the dye laser with the DCM dye dissolved in methanol and frequency doubled with a BBO crystal. The dye laser wavelength was monitored by a spectrometer (Ocean Optics, HR2000) equipped with a 600 lines/mm grating. The wavelength calibration was achieved by simultaneously recording the output from the discharge cell, the optogalvanic spectra of neon from a hollow cathode lamp and fringes from a 1 mm thick fused silica Fabry-Perot etalon (FSR 3.33 cm^{-1}) via three boxcar averagers (SR 250). The optogalvanic signals from the neon hollow cathode lamp provided well distributed spectral lines of neon in the region of interest, listed in the MIT table [27], that serve as wavelength standards. The interference fringes from the etalon were used to interpolate between the neon lines. The spectrum was recorded with a scanning step of 0.05 cm^{-1} of the dye laser. From the location of the peak signal positions, the transition energies have been determined within an accuracy of $\pm 0.2\ \mathrm{cm}^{-1}$.

For the measurement of the photoionization cross section, the intensity of the ionizing laser was varied by inserting the neutral density filters (Edmund Optics) and on each insertion the energy was measured with an energy meter (R-752, Universal Radiometer). The variation in the amplitude of the ionization signal with the laser intensity was recorded using a 200 MHz digital storage oscilloscope (TDS 2024) and a computer through RS232 interface. The ionizing wavelengths at 312 nm, 300 nm, 290 nm, 280 nm, and 270 nm, used in the present experiment, were achieved by charging the PDL-2 dye laser with the dyes DCM, Rhodamine 610, Rhodamine 590, and Fluorescence 548 dissolved in methanol and frequency doubled with a BBO crystal. The ionizing wavelength at 266 nm was achieved by frequency doubling the second-harmonic generation (SHG) of the Nd:YAG laser.

III. RESULTS AND DISCUSSION

The excitation and/or ionization scheme for the measurement of the optical oscillator strength distribution in the discrete and continuous spectrum of helium is shown in Fig. 2. The ground state of helium is $1s^2\ ^1S_0$ and the $2s\ ^1S_0$ metastable state becomes significantly populated in a low-pressure glow discharge via collisional processes. The highly excited Rydberg states of helium and the near threshold region can be easily accessed from this metastable state with tunable uv lasers using laser optogalvanic effect [28,29]. Babin *et al.* [30] used a hollow cathode discharge cell to measure the photoionization cross sections of refractory elements. Stockhausen *et al.* [31] used a hollow cathode lamp to measure the photoionization cross section of the autoionizing lines of copper. The optogalvanic method, in conjunction with hollow cathode discharges, has also been used for the study of the photoionization processes in complex atoms [32].

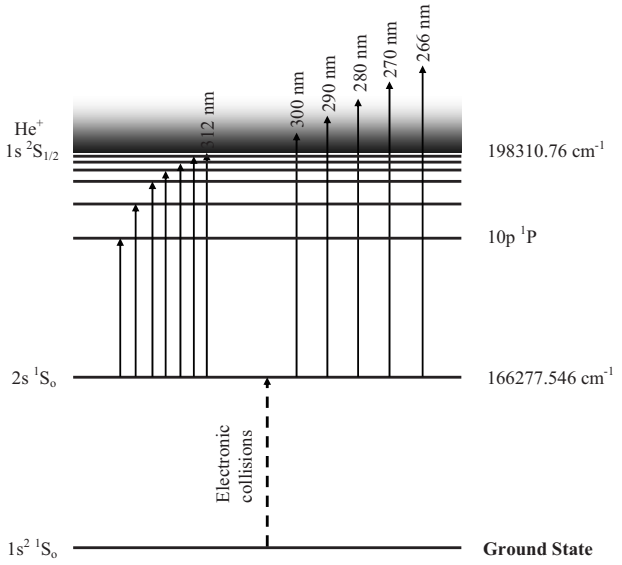

FIG. 2. Energy level diagram for the measurement of the oscillator strength for the $2s\ ^1S \rightarrow np\ ^1P$ $(10 \leqslant n \leqslant 52)$ Rydberg transitions of helium. The level energies are taken from Martin [52].

The discrete absolute oscillator strengths (f values) for the high lying members of the $2s\ ^1S \rightarrow np\ ^1P$ Rydberg series have been determined with the experimental technique developed by Mende and Kock [33]. We have recently exploited this technique to measure the optical oscillator strengths of the autoionizing resonances in neon [34] and to determine the oscillator strength distribution in lithium [35]. A simplified relation between the f values of the Rydberg transitions and the photoionization cross section measured at the ionization threshold is given as [33]

$$f_n = \frac{4\varepsilon_0 mcS^n \lambda^+}{e^2 S^+ \lambda_n} \sigma(\lambda^+). \tag{1}$$

Here f_n is the oscillator strength for the nth transition of a Rydberg series, which is directly proportional to the photoionization cross section $\sigma(\lambda^+)$ measured at wavelength λ^+, i.e., at the ionization threshold. Also, S^+ is the ion signal at the ionization threshold and S^n is the integrated ion signal intensity for the nth transition. The constants m, e, c, and ε_0 are the mass of electron, the charge on electron, speed of light, and the permittivity of free space, respectively.

The oscillator strength f_n in the discrete spectrum merges into the differential oscillator strength df/dE in the continuous spectrum, which are related as [5]

$$\frac{(n^*)^3 f_n}{2R} = \frac{df}{dE}. \tag{2}$$

Here, n^* is the effective quantum number, R is the Rydberg constant, and E is the photon energy. The spectral density of oscillator strength is also related to the photoionization cross section as [5]

$$\frac{df}{dE} = 9.11 \times 10^{15}\ \sigma(E)\ \text{cm}^{-2}\ (\text{eV})^{-1}. \tag{3}$$

The photoionization cross sections from the $2s\ ^1S_0$ excited state of helium at and above the first ionization threshold $\sigma(\lambda^+)$ and $\sigma(E)$, respectively, have been determined using the saturation technique as described by Burkhardt *et al.* [36], He *et al.* [37], and Saleem *et al.* [38]. This technique has been widely used for the measurement of the photoionization cross sections of the excited states of alkali, alkaline earths, and rare gas atoms ([36–40], and references therein). We have applied the saturation technique to determine the photoionization cross sections of the excited states of the helium [41] in a dc discharge and that of lithium [42] using the thermionic diode ion detector.

In the photoionization process, ions are produced which are detected as a voltage across a load resistor. A relation between the total charge Q per pulse and the photoionization cross section, ignoring the spontaneous emission, can be written as [36,38]

$$Q = eN_{ex}V_{vol}\left[1 - \exp\left(-\frac{\sigma U}{2\hbar\omega A}\right)\right]. \tag{4}$$

Here e is the electronic charge, N_{ex} is the density of the excited atoms, A is the cross-sectional area of the ionizing laser beam, U is the total energy per pulse of the ionizing laser, V_{vol} is the interaction volume, and σ is the absolute cross section for photoionization. This equation holds with the assumption that the intensity of the ionizing laser is much higher, i.e., in excess to that required for saturating the resonance transition; also the transition remains saturated during the laser pulse and the laser beam is uniform and linearly polarized. The accurate determination of the photoionization cross section σ requires accurate measurement of the ionizing laser energy as well as the characterization of the spatial profile of the ionizing laser pulse in the interaction region. The uncertainty in the energy determination is mainly due to the energy fluctuations in the Nd:YAG laser (±5%) and in the measuring instrument (±3%). To characterize the ionizing laser's spatial profile, a beam splitter was placed before the entrance of the discharge cell and a small fraction of the laser beam was used to reproduce its spatial profile at the interaction region. The spatial profile of the ionizing laser was generated by scanning a PIN photodiode across its diameter. The intensity distribution of the laser beam was found to be Gaussian and its spot size was determined at the point where the irradiance (intensity) falls to $1/e^2$ of its axial value. A lens of 50 cm focal length was used in the path of the ionizing laser to meet the power requirement for saturation. The area of the overlap region in the confocal limit was calculated using the following relation [43,44]

$$A = \pi\gamma_0^2\left[1 + \left(\frac{\lambda_{io}\ell}{\pi\gamma_0^2}\right)^2\right]. \tag{5}$$

Here "ℓ" is the distance on the beam propagation axis from the focus and $\gamma_0 = f\lambda_{io}/\pi\gamma_s$ is the beam waist at $\ell = 0$, γ_s is half the spot size of the ionizing laser beam on the focusing lens, f is the focal length, and λ_{io} is the wavelength of the ionizing laser.

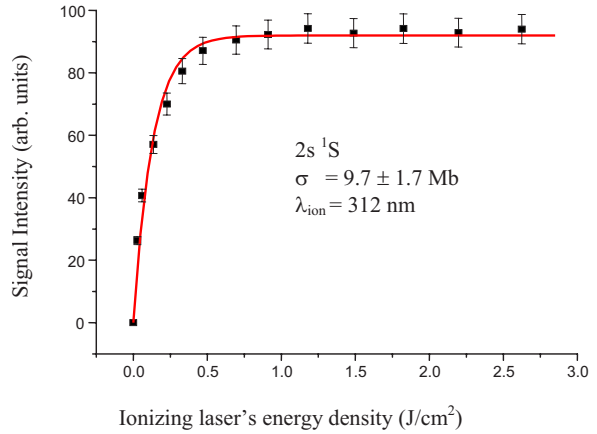

FIG. 3. (Color online) The photoionization data for the $2s\ ^1S$ excited state of helium at the ionization threshold with the ionizing laser set at 312 nm. The solid line is the least squares fit to Eq. (4) to the observed data for extracting the photoionization cross section. The error limits on the data result from pulse-to-pulse fluctuations in the optogalvanic signal.

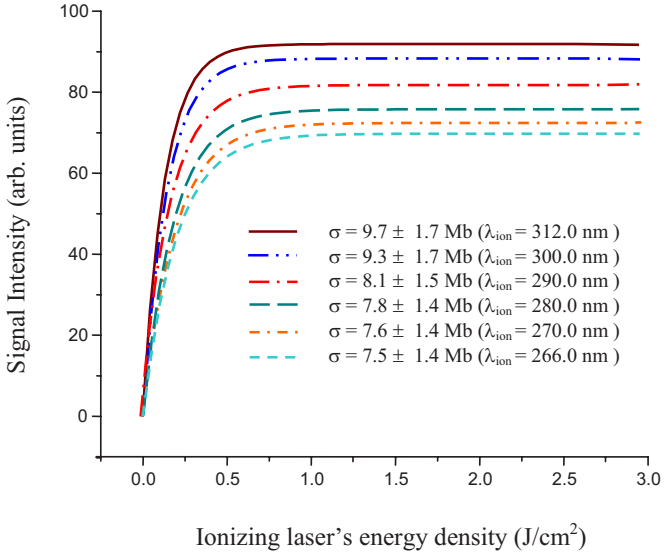

FIG. 4. (Color online) The fitted curves to the experimental data verses the energy density of the ionizing laser for the photoionization cross section from the $2s\ ^1S$ excited state of helium at threshold (312 nm), at 300 nm, at 290 nm, at 280 nm, at 270 nm, and at 266 nm. These fitted curves are used to extract the photoionization cross sections of the $2s\ ^1S$ excited state.

The absolute measurements of the photoionization cross sections requires that there must be a linear relation between the number of photoionized electrons and the measured optogalvanic voltage change. We ensured the linear operation of the rf discharge for the strongest optogalvanic signal corresponding to the maximum available ionizing laser intensity. The discharge conditions were also optimized to saturate the $2s\ ^1S$ metastable state and also to achieve the maximum ionization efficiency for the high lying Rydberg states of helium. Moreover, the energy difference between the first ionization threshold and the 22 ^1P Rydberg level is $\approx$0.028 eV, which is comparable to kT (thermal energy) in the present experimental conditions. This complements the maximum ionization efficiency of the $n\ ^1P$ Rydberg states with $n \geqslant 22$.

In order to determine the photoionization cross section $\sigma(\lambda^+)$ at threshold, the electrons from the collisionally populated $2s\ ^1S$ metastable state were promoted to the first ionization threshold by the direct absorption of the 312 nm laser. The intensity of the ionizing laser was varied using the neutral density filters and the corresponding optogalvanic signals were recorded on a storage oscilloscope. The variation in the amplitude of the optogalvanic signal was plotted as a function of intensity of the ionizing laser. A typical experimental curve for the photoionization from the $2s\ ^1S$ excited state of helium at the first ionization threshold is presented in Fig. 3. Evidently, the optogalvanic signal first increases linearly with the laser intensity and then stops to increase further, i.e., the signal becomes saturated. The solid line that passes through the experimental data points is the least squares fit to Eq. (4). The photoionization cross section from the $2s\ ^1S$ metastable state at the ionization threshold has been determined from this fitting procedure as 9.7±1.7 Mb. This value of the threshold cross section is in excellent agreement with the experimental work of Stebbings *et al.* [45] and the theoretical work of Burgess and Seaton [46], Norcross [47], Jacobs [48], Chang and Zhen [49], and Chang and Fang [50]. The measured value of the photoionization cross section (9.7±1.7 Mb) from the $2s\ ^1S$ excited state at the first ionization threshold was then used to extract the f values of the $2s\ ^1S \rightarrow np\ ^1P$ Rydberg series of helium.

In order to find the spectral density of oscillator strengths corresponding to the $2s\ ^1S$ excited state the photoionization cross sections from the $2s\ ^1S$ state were measured at five ionizing laser wavelengths 300 nm, 290 nm, 280 nm, 270 nm, and 266 nm, above the first ionization threshold. The photoionization cross sections at these ionizing laser wavelengths have also been determined using the saturation technique. Figure 4 shows the variation of the photoion signals as a function of intensity of the ionizing laser for the six ionizing lasers at threshold (312 nm), at 300 nm, 290 nm, 280 nm, 270 nm, and 266 nm. Each curve is a least squares fit of Eq. (4) to the experimental data points. The measured values of the photoionization cross section from this fitting procedure along with the earlier experimental and theoretical work are shown in Fig. 5 and also tabulated in Table I. The solid line is the work of Jacobs [48], the dash-dotted line is from Norcross [47], and the dashed line is the results of Burgess and Seaton [46]. The closed circles are the experimental points of Stebbings *et al.* [45] who used the saturation technique to determine the photoionization cross section of helium $2s\ ^1S$ metastable state above the first ionization threshold corresponding to 23 different ionizing laser wavelengths. The calculated values of the photoionization cross section from the $2s\ ^1S$ metastable state of helium at threshold [50] and at the ionizing wavelengths of 300 nm and 280 nm [20] are also shown in Fig. 5. The work of Stebbings *et al.* [45] is the only experimentally reported values of the photoionization cross section from the $2s\ ^{1,3}S$ metastable states. Our measured values of the cross section are 9.7 Mb, 9.3 Mb, 8.1 Mb, 7.8 Mb, 7.6 Mb, and 7.5 Mb at threshold and at excess photon energies of 0.16 eV, 0.3 eV, 0.46 eV,

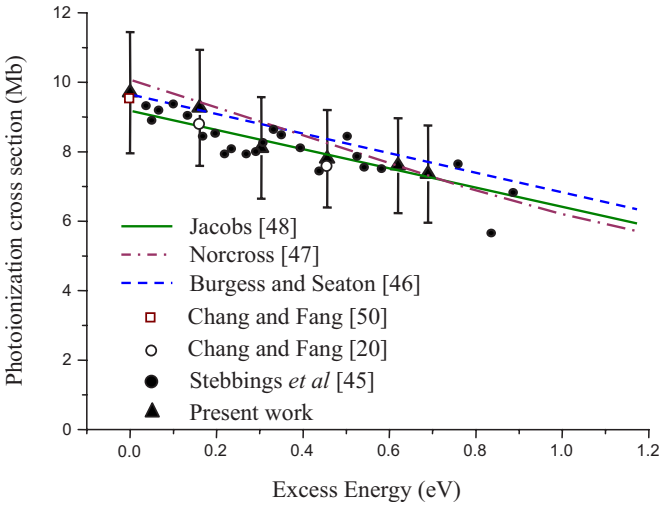

FIG. 5. (Color online) Comparison of the experimentally measured values of the absolute photoionization cross section from the $2s\ ^1S$ excited state with the earlier experimental and theoretical work.

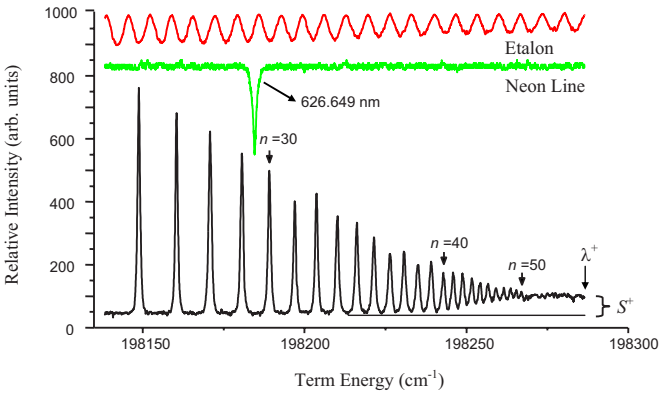

FIG. 6. (Color online) A portion of the $2s\ ^1S \rightarrow np\ ^1P$ ($26 \leqslant n \leqslant 52$) Rydberg series of helium.

0.62 eV, and 0.69 eV, respectively, above the first ionization threshold. These values are in excellent agreement to the earlier reported work. It is apparent that the photoionization cross section from the $2s\ ^1S$ excited state decreases linearly with an increase in the photon energy in the measured energy range.

In the next step, we have recorded the $2s\ ^1S \rightarrow np\ ^1P$ ($10 \leqslant n \leqslant 52$) Rydberg series of helium to find the values of the remaining parameters λ_n, λ^+, S^+, and S^n used in Eq. (1). The above mentioned Rydberg series was recorded by scanning the dye laser from 325 nm to 312 nm. A portion of the recorded Rydberg series from $n=26$ to $n=52$ is shown in Fig. 6. The top trace is the etalon fringes and the middle trace is the wavelength calibration spectrum of neon. The absolute oscillator strengths (f values) for the $2s\ ^1S \rightarrow np\ ^1P$ Rydberg transitions from $n=10$ to $n=52$ were then determined using Eq. (1). The extracted values of the absolute oscillator strengths along with the corresponding wavelengths for the $2s\ ^1S \rightarrow np\ ^1P$ ($10 \leqslant n \leqslant 52$) Rydberg series are listed in Table II.

The measured oscillator strengths are plotted against the principal quantum number "n" in Fig. 7. The solid line that passes through the experimental data points is the least squares fit to the equation:

$$\sigma = Kn^{-\alpha}. \tag{6}$$

Here σ is the photoabsorption cross section; K and α are constants. This indicates a smooth decrease of the f values as $n^{-2.93}$. However, for an unperturbed Rydberg series the f values for the successive Rydberg transitions fall off as n^{-3} [5]. The measured f values are reasonably close to this hydrogenic limit within the experimental error. The slight deviation may arise due to field effects and consequently a small increase in the broadening and energy shift of the high lying members of the series close to the series limit may occur. A net electric field of ≈ 2 V/cm in the rf discharge, calculated from the series termination in our earlier work [23], may be responsible for this broadening and shift. We have calibrated f values of the Rydberg series using Eq. (1). This equation shows direct dependence of f values on the integrated line intensity (product of signal height and the line width) and the transition energies of the observed Rydberg transitions. The small electric field (≈ 2 V/cm) generates very little energy shift, broadening, and also depresses the signal height of the highly excited states. The error introduced in the f values due to this field effect is negligibly small, which does not significantly affects the 20% uncertainty in the measured f values. The measured f values of the $2s\ ^1S \rightarrow np\ ^1P$ ($10 \leqslant n \leqslant 52$) Rydberg series together with the calculated oscillator

TABLE I. Present experimental data for the absolute photoionization cross section from the $2s\ ^1S$ excited state of helium and some of the previous theoretical work.

	Present work			Previous work
State	Wavelength (nm)	Cross section (Mb)	$\left(\frac{df}{dE}\right)_E$ (eV^{-1})	Cross section (Mb)
$2s\ ^1S_0$	312	9.7±1.7	0.08837±(18%)	9.473 [45]
	300	9.3±1.7	0.08472±(18%)	8.707 [20]
	290	8.1±1.5	0.07379±(18%)	
	280	7.8±1.4	0.07106±(18%)	7.833 [20]
	270	7.6±1.4	0.06924±(18%)	
	266	7.5±1.4	0.06833±(18%)	

TABLE II. Excitation wavelengths and the oscillator strengths for the $2s\ ^1S \rightarrow np\ ^1P$ Rydberg series of helium.

n	Wavelength (nm)	Oscillator strength (±20%)
10	323.22	2.24×10^{-3}
11	321.25	1.87×10^{-3}
12	319.77	1.45×10^{-3}
13	318.62	1.10×10^{-3}
14	317.72	8.84×10^{-4}
15	316.99	7.64×10^{-4}
16	316.40	6.20×10^{-4}
17	315.92	4.76×10^{-4}
18	315.51	4.47×10^{-4}
19	315.16	3.51×10^{-4}
20	314.87	3.22×10^{-4}
21	314.62	2.59×10^{-4}
22	314.40	2.38×10^{-4}
23	314.21	1.71×10^{-4}
24	314.04	1.73×10^{-4}
25	313.89	1.56×10^{-4}
26	313.76	1.40×10^{-4}
27	313.65	1.33×10^{-4}
28	313.54	1.10×10^{-4}
29	313.45	8.53×10^{-5}
30	313.37	9.40×10^{-5}
31	313.29	8.46×10^{-5}
32	313.22	7.85×10^{-5}
33	313.16	6.94×10^{-5}
34	313.10	5.37×10^{-5}
35	313.05	5.51×10^{-5}
36	313.00	5.41×10^{-5}
37	312.96	4.52×10^{-5}
38	312.92	4.60×10^{-5}
39	312.88	3.95×10^{-5}
40	312.84	3.76×10^{-5}
41	312.81	3.20×10^{-5}
42	312.78	2.88×10^{-5}
43	312.75	2.80×10^{-5}
44	312.73	2.81×10^{-5}
45	312.70	2.18×10^{-5}
46	312.68	2.24×10^{-5}
47	312.66	2.01×10^{-5}
48	312.64	1.93×10^{-5}
49	312.62	2.04×10^{-5}
50	312.60	1.94×10^{-5}
51	312.58	1.70×10^{-5}
52	312.57	1.75×10^{-5}

strengths [11] for the same series from $n=2-10$ are also plotted against the principal quantum number "n" in Fig. 8. Our measured f value for $n=10$ is 0.002 24, which is in excellent agreement with the calculated value of 0.002 23 [11].

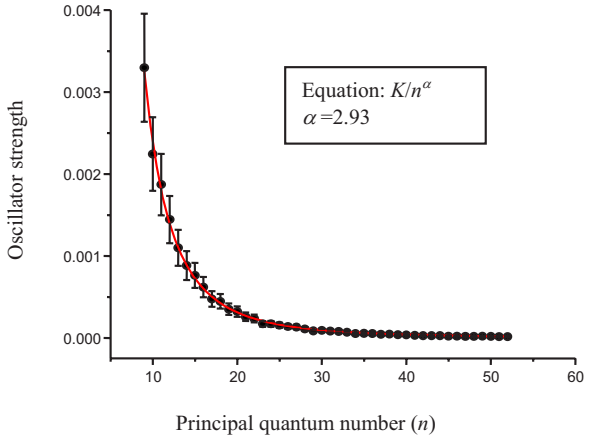

FIG. 7. (Color online) A plot of the optical oscillator strengths of the $2s\ ^1S \rightarrow np\ ^1P$ ($10 \leqslant n \leqslant 52$) Rydberg series of helium versus the principal quantum number.

After the determination of f values in the discrete region the measurements were extended to the ionization continuum. The densities of oscillator strength were then estimated, using Eq. (3), from the measured values of the photoionization cross section at the excess photon energies of 0.0, 0.16 eV, 0.3 eV, 0.46 eV, 0.62 eV, and 0.69 eV above the ionization threshold, and are tabulated in Table I. In order to give an overall view of the oscillator strength distribution of the helium spectrum, we have plotted the oscillator strengths f_n in the discrete spectrum and the related oscillator strength density df/dE in the continuum on the same graph in Fig. 9. The solid line is a linear fit to the experimental data points just to show the trend of the oscillator strength distribution in the discrete and continuum regions, while the dashed line represents the ionization threshold. Figure 9 clearly indicates a smooth merging of the discrete absorption features into the continuous absorption across the ionization threshold. The

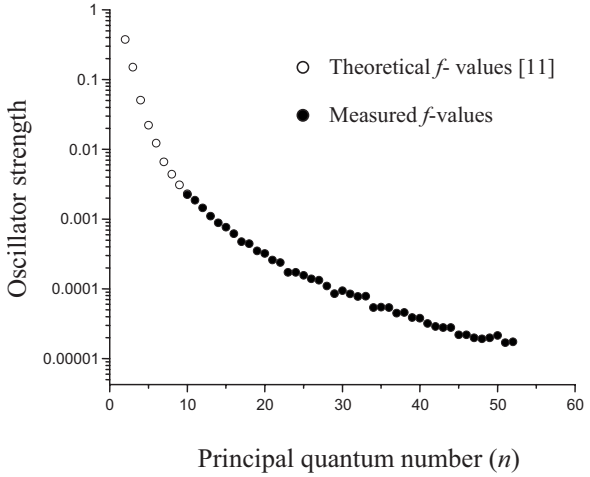

FIG. 8. The experimental and theoretical oscillator strengths of the $2s\ ^1S \rightarrow np\ ^1P$ Rydberg transitions of helium versus the principal quantum number. The theoretical values [11] for ($2 \leqslant n \leqslant 10$) and the measured values for ($10 \leqslant n \leqslant 52$).

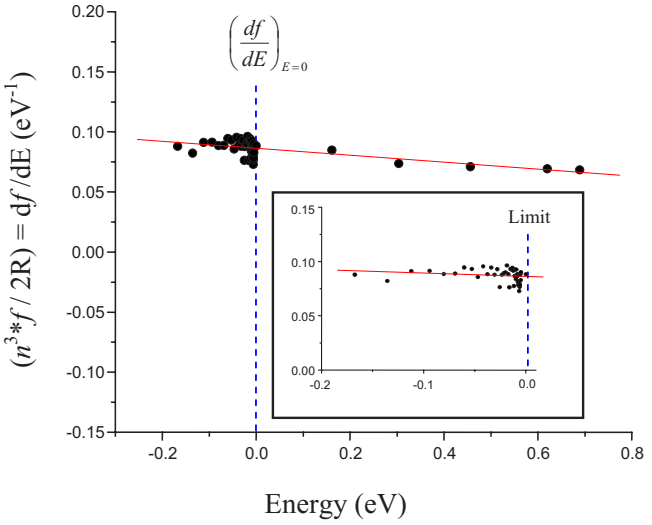

FIG. 9. (Color online) The experimentally measured oscillator strength distribution in the discrete and the continuous spectrum of helium.

inset in the figure shows an expanded view of the discrete region from the threshold up to −0.2 eV. The figure also discards the existence of the Cooper minima in the cross section within our measurement energy range from −0.2 eV to 0.7 eV.

The maximum overall uncertainty in the determination of the absolute photoionization cross section is estimated to be 18% [51], which is attributed to the experimental errors in the measurements of the laser energy, the cross-sectional area of the laser beam at the focusing volume, the calibration of the detection system and a nonuniform transmission of the quartz windows. The uncertainty in the measurements of the f values is about 20%, which is attributed to additional errors in the measurements of the transition energy and the transition width measurements.

In conclusion, we have experimentally determined the oscillator strength distribution both in the discrete and in the continuous spectrum of helium using the $2s\ ^1S_0$ excited state. Continuity across the ionization threshold has been found. This type of connection has been experimentally explored. This technique can be extended to determine the oscillator strength distribution in the discrete and the continuous spectra of other inert gases. Further work in this direction is in progress in our laboratory.

ACKNOWLEDGMENTS

The authors are grateful to the Higher Education Commission (HEC), Pakistan Science Foundation (PSF), and the Quaid-i-Azam University, Islamabad, Pakistan for financially supporting the present research work.

[1] U. Fano and J. W. Cooper, Rev. Mod. Phys. **40**, 441 (1968).
[2] M. Inokuti, Rev. Mod. Phys. **43**, 297 (1971).
[3] G. W. F. Drake, *Atomic, Molecular, & Optical Physics Handbook* (AIP Press, New York, 1996).
[4] M. C. E. Huber and R. J. Sandeman, Rep. Prog. Phys. **49**, 397 (1986).
[5] J. Berkowitz, *Photoabsorption, Photoionization and Photoelectron Spectroscopy* (Academic Press, New York, 1979); *Atomic and Molecular Photoabsorption, Absolute Total Cross Sections* (Academic Press, New York, 2002).
[6] W. F. Chan, G. Cooper, K. H. Sze, and C. E. Brion, J. Phys. B **23**, L532 (1990).
[7] W. F. Chan, G. Cooper, and C. E. Brion, Phys. Rev. A **44**, 186 (1991).
[8] F. B. Dunning and R. F. Stebbings, Phys. Rev. Lett. **32**, 1286 (1974).
[9] L. C. Green, N. C. Johnson, and E. K. Kolchin, Phys. Rev. **139**, A373 (1965).
[10] L. C. Green, N. C. Johnson, and E. K. Kolchin, Astrophys. J. **144**, 369 (1966).
[11] W. L. Wiese, M. W. Smith, and B. M. Glennon, *Atomic Transition Probabilities: Volume I Hydrogen Through Neon* (NSRDS-NBS, Washington, DC, 1966).
[12] B. Schiff, C. L. Pekeris, and Y. Accad, Phys. Rev. A **4**, 885 (1971).
[13] K. R. Devine and L. Stewart, J. Phys. B **5**, 2182 (1972).
[14] M. Y. Amusia and N. A. Cherepkov, Phys. Rev. A **13**, 1466 (1976).
[15] B. F. Davis and K. T. Chung, Phys. Rev. A **25**, 1328 (1982).
[16] A. Kono and S. Hattori, Phys. Rev. A **29**, 2981 (1984).
[17] A. Kono and S. Hattori, Phys. Rev. A **30**, 2093 (1984).
[18] J. A. Fernley, K. T. Taylor, and M. J. Seaton, J. Phys. B **20**, 6457 (1987).
[19] M. K. Chen, J. Phys. B **27**, 865 (1994).
[20] T. N. Chang and T. K. Fang, Phys. Rev. A **52**, 2638 (1995).
[21] M. A. Dillon and M. Inokuti, J. Chem. Phys. **74**, 6271 (1981).
[22] J. Berkowitz, J. Phys. B **30**, 881 (1997).
[23] S. Hussain, M. Saleem, N. M. Shaikh, and M. A. Baig, J. Phys. D **39**, 3788 (2006).
[24] B. N. Ganguly and A. Garscadden, Appl. Phys. Lett. **46**, 540 (1985).
[25] M. A. Zia and M. A. Baig, Eur. Phys. J. D **28**, 323 (2004).
[26] R. D. May and P. H. May, Rev. Sci. Instrum. **57**, 2242 (1985).
[27] G. R. Harrison, *M. I. T. Wavelength Tables* (MIT, Cambridge, England, 1982).
[28] B. Barieri and N. Beverini, Rev. Mod. Phys. **62**, 603 (1990).
[29] D. H. Katayama, M. J. Cook, V. E. Bondybey, and T. A. Miller, Chem. Phys. Lett. **62**, 542 (1979).
[30] F. Babin and J.-M. Gagné, J. Phys. B **54**, 35 (1992).
[31] G. Stockhausen, W. Mende, and M. Kock, J. Phys. B **29**, 665 (1996).
[32] S. Lévesque, J.-M. Gagné, and F. Babin, J. Phys. B **30**, 1331 (1997).
[33] W. Mende and M. Kock, J. Phys. B **29**, 655 (1996).
[34] S. Mahmood, N. Amin, Sami-ul-Haq, N. M. Shaikh, S. Hussain, and M. A. Baig, J. Phys. B **39**, 2299 (2006).

[35] S. Hussain, M. Saleem, and M. A. Baig, Phys. Rev. A **75**, 022710 (2007).
[36] C. E. Burkhardt, J. L. Libbert, Jian Xu, J. J. Leventhal, and J. D. Kelley, Phys. Rev. A **38**, 5949 (1988).
[37] L. W. He, C. E. Burkhardt, M. Ciocca, J. J. Leventhal, and S. T. Manson, Phys. Rev. Lett. **67**, 2131 (1991).
[38] M. Saleem, S. Hussain, M. Rafiq, and M. A. Baig, J. Phys. B **39**, 5025 (2006).
[39] N. Amin, S. Mahmood, M. Anwar-ul-Haq, M. Riaz, and M. A. Baig, Eur. Phys. J. D **37**, 23 (2006).
[40] M. Saleem, N. Amin, S. Hussain, M. Rafiq, S. Mahmood, and M. A. Baig, Eur. Phys. J. D **38**, 277 (2006).
[41] S. Hussain, M. Saleem, M. Rafiq, and M. A. Baig, Phys. Rev. A **74**, 022715 (2006).
[42] S. Hussain, M. Saleem, and M. A. Baig, Phys. Rev. A **74**, 052705 (2006).
[43] W. Demtroder, *Laser Spectroscopy* (Springer, Berlin, 1996).
[44] J. M. Song, T. Inoue, H. Kawazumi, and T. Ogawa, Anal. Sci. **15**, 601 (1999).
[45] R. F. Stebbing, F. B. Dunning, F. K. Tittel, and R. D. Rundel, Phys. Rev. Lett. **30**, 815 (1973).
[46] A. Burgess and M. J. Seaton, Mon. Not. R. Astron. Soc. **120**, 121 (1960).
[47] D. W. Norcross, J. Phys. B **4**, 652 (1971).
[48] V. L. Jacobs, Phys. Rev. A **4**, 939 (1971).
[49] T. N. Chang and M. Zhen, Phys. Rev. A **47**, 4849 (1993).
[50] T. N. Chang and T. K. Fang, Phys. Rev. A **52**, 2052 (1995).
[51] J. Topping, *Errors of Observation and their Treatment* (Chapman and Hall, London, 1962).
[52] W. C. Martin, J. Phys. Chem. Ref. Data **2**, 257 (1973).